

Room-Temperature Red–Green–Blue Whispering-Gallery Mode Lasing and White-Light Emission from Cesium Lead Halide Perovskite (CsPbX_3 , $X = \text{Cl, Br, I}$) Microstructures

Pengfei Guo, Mohammad Kamal Hossain, Xia Shen, Haibin Sun, Wenchao Yang, Chaoping Liu, Chun Yuen Ho, Cheuk Kai Kwok, Sai-Wing Tsang, Yongsong Luo, Johnny C. Ho, and Kin Man Yu*

Wavelength-tunable nano/microlasers are essential components for various highly integrated and multifunctional photonic devices. Based on the different band gap/composition of inorganic cesium lead halide perovskite materials, broad band light absorption and emission devices can be achieved. Herein, a vapor–liquid–solid route for growing cesium lead halide perovskite (CsPbX_3 , $X = \text{Cl, Br, I}$) microcrystal structures is demonstrated. These square-shaped microstructures exhibit strong blue, green, and red photoluminescence, indicating that their band gaps can be engineered to cover the entire visible range. Optically pumped red–green–blue whispering-gallery mode lasers based on the controlled composition of these microcrystals are successfully realized at room temperature. Moreover, rationally designed white-light-emitting chips with high brightness are fabricated utilizing these metal halide perovskite microstructures grown on sapphire. All these results evidently suggest a feasible route to the design of red–green–blue lasers and white-light emitters for potential applications in full-color displays as well as photonic devices.

1. Introduction

A rational design and construction of white-light-emitting components based on semiconductor materials are extremely important in lighting and display technologies.^[1–4] In general, there are two reasonable approaches developed to realize the white light source. They are the synthesis of semiconductor alloy nanostructures with widely tunable band gaps,^[5–7] and the construction of a white lighting emitter with various single band gap semiconductors that have monochromatic luminescence with high quantum efficiency.^[8–10] However, white light generated from red–green–blue emitters based on semiconductor nanostructures has been known as the major challenge in the solid-state lighting community.^[1,2,8,9] For example, a suitable mix for white-light radiation with favorable wavelengths and inten-

sity ratios, proper color rendering index, and high stability is still lacking.^[11,12] Recently, perovskite materials have brought a variety of new opportunities for the advancement of nanophotonics and optoelectronics.^[13–23] In particular, inorganic metal halide perovskites, such as cesium lead halide perovskites, have drawn enormous attention because they show great promises for various photoelectric applications, such as the natural high-quality whispering-gallery-mode (WGM) or Fabry–Perot (F–P) resonators,^[16,17,24–26] laser cooling,^[18] solar cells,^[27–30] and light emitting diodes.^[31–33] Moreover, they also exhibit a broad band gap tunability for multifunctional devices and circuits covering the entire visible spectrum.^[19,20] Therefore, these unusual semiconductor materials may offer the opportunity to design novel white-light-emitting devices in future full-color displays.


Currently, solution-based synthesis methods have been commonly used to realize the band gap-tunable cesium lead halide perovskite (CsPbX_3 , $X = \text{Cl, Br, I}$) quantum dots.^[34–37] Protesescu et al. reported a new avenue for the growth of CsPbX_3 perovskite nanocrystals by the solution phase method, which shows bright emissions with a wide color gamut.^[38] In comparison, chemical vapor deposition (CVD) is another attractive approach for the synthesis of diverse

Dr. P. F. Guo, M. K. Hossain, Dr. C. P. Liu, C. Y. Ho, C. K. Kwok, Prof. K. M. Yu
Department of Physics
City University of Hong Kong
Kowloon, Hong Kong, China
E-mail: kinmanyu@cityu.edu.hk

Dr. P. F. Guo, Dr. X. Shen, Dr. H. B. Sun, Dr. W. C. Yang, Prof. Y. S. Luo
Key Laboratory of Microelectronic and Energy of Henan Province
School of Physics and Electronic Engineering
Xinyang Normal University
Xinyang 464000, China

Dr. P. F. Guo
Department of Materials Science and Engineering
Hunan University
Changsha 410082, China

Dr. S.-W. Tsang, Prof. J. C. Ho
Department of Materials Science and Engineering
City University of Hong Kong
Kowloon, Hong Kong, China

 The ORCID identification number(s) for the author(s) of this article can be found under <https://doi.org/10.1002/adom.201700993>.

DOI: 10.1002/adom.201700993

low-dimensional nanostructures with advantages of simple setup, low cost, easy operation, and high yield.^[39–43] Particularly, the CVD approach involving the evaporation of solid precursors has been especially popular because of its flexibility for a wide range of material syntheses. For example, various inorganic perovskite nanostructures have been realized via this CVD approach, acting as nanoscale lasers,^[44,45] light emitting diodes (LEDs),^[46] and solar cells.^[47] Very recently, the composition-tunable perovskite CsPbX₃ nanowires have also been achieved, which can be functioned as effective Fabry–Perot resonators with emissions from 415 to 673 nm.^[22] However, to the best of our knowledge, white-light-emitting chips based on the all-inorganic high-quality metal halide perovskite microcrystals, which may have wider potential applications, have not yet been demonstrated.

In this work, we report the synthesis of crystalline CsPbX₃ (X = Cl, Br, I) microcrystals by a simple CVD method. Detailed investigation shows that these microcrystals have excellent crystallinity, exhibiting strong blue, green, and red emissions with band gaps covering the entire visible range. In addition, room temperature red–green–blue WGM lasers based on these CsPbX₃ microstructures are readily achieved by pumping with a 355 nm pulsed laser. Moreover, high brightness white-light-emitting chips have also been fabricated based on these metal halide perovskite microcrystals. All these results evidently suggest a feasible route to the rational design of red–green–blue lasers and white-light emitters, which have promising applications in the next-generation full-color displays and integrated photonic devices.

2. Results and Discussion

Generally, low and high resolution scanning electron microscopy (SEM) images reveal that CsPbCl₃ microstructures synthesized by our CVD method (see the Experimental Section) are square-like crystals with a side length of several micrometers (Figure 1A,B) and a thickness of several hundreds of nanometers (Figure S1, Supporting Information). Figure 1C shows an X-ray diffraction (XRD) pattern of CsPbCl₃ microstructures, which can be indexed to the tetragonal phase. Microstructures of CsPbBr₃ and CsPbI₃ with similar morphology were also prepared via the same CVD method and their SEM micrographs and XRD patterns are shown in Figure S2 (Supporting Information). Unlike CsPbCl₃, CsPbBr₃ and CsPbI₃ microstructures are indexed to the monoclinic and orthorhombic phases, respectively. The size distributions of the CsPbCl₃, CsPbBr₃, and CsPbI₃ microcrystals (see Figure S3, Supporting Information) depicted in Figure 1D reveal that the average size of CsPbI₃, CsPbBr₃, and CsPbCl₃ microcrystals is about 2, 6, and 3 μm, respectively. Notably, these distributions were obtained by measuring more than 400 microcrystals in each sample group. It can be anticipated that all these CsPbX₃ microcrystals are formed during the self-assembly random process. Since the CsPbX₃ (X = Cl, Br, I) crystals underwent a phase transition from cubic to tetragonal (CsPbCl₃), monoclinic (CsPbBr₃), and orthorhombic (CsPbI₃), respectively, at the temperature of 47, 130, and 328 °C.^[48] The well-defined square-like morphology of all these microstructures may originate from their cubic phase at high temperature during growth.^[48,49]

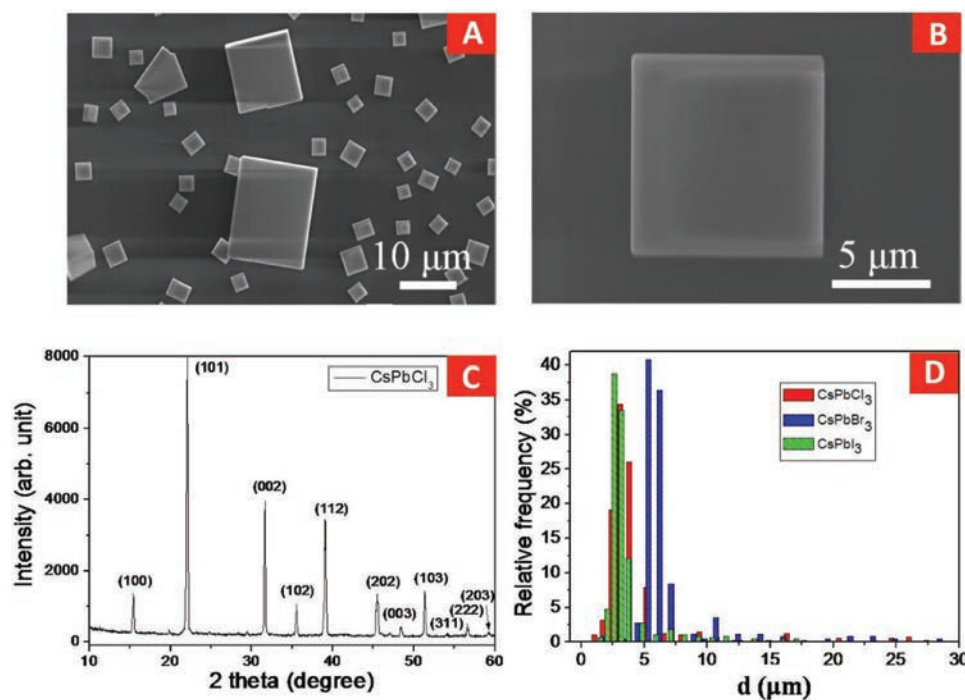


Figure 1. A) A low-magnification and B) a high-magnification SEM image, and C) an XRD pattern of as-grown CsPbCl₃ microstructures. D) Size distributions for the CsPbCl₃, CsPbBr₃, and CsPbI₃ microcrystal samples as shown in Figure S1 (Supporting Information). These data were gathered by counting more than 400 microcrystals from the SEM images in each sample group.

At the same time, the composition of these microstructures was measured by energy-dispersive X-ray spectroscopy (EDX) analysis. **Figure 2A–C** shows the EDX spectra of these microstructures. Specifically, the atomic ratios of each constituent are measured to be [Cs:Pb:Cl = 17.0:18.7:64.3, Cs:Pb:Br = 18.1:18.1:63.8, and Cs:Pb:I = 18.4:18.3:63.3]. These atomic ratios are in good agreement with the expected 1:1:3 ratio for Cs:Pb:X (X = Cl, Br, I), indicating that the microstructures are indeed CsPbCl₃, CsPbBr₃, and CsPbI₃, respectively. The corresponding elemental mapping images of these typical CsPbX₃ microstructures are shown in **Figure 2D–F**, which clearly reveal the homogeneous atomic distributions throughout the entire squares. No detectable amount of other impurities or noticeable clusterings can be observed within these structures. Results shown in **Figure 2D–F** suggest that these structures are indeed random ternary semiconductor alloys. As an example, **Figure 2G** shows a low-magnification transmission electron microscope (TEM) image of CsPbBr₃ microcrystals that were randomly dispersed on a copper grid. The inset of **Figure 2G** displays a typical TEM image of a single CsPbBr₃ crystal with the side length of ≈3 μm. The corresponding selected area electron diffraction (SAED) pattern shown in **Figure 2H** indicates that these CsPbBr₃ microcrystals are single crystalline with the monoclinic structure.

To shed light on their optical properties, **Figure 3A,D,G** gives the top-view real-color images of perovskite CsPbX₃ (X = Cl, Br, I) microcrystals grown on Si/SiO₂ substrates under a continuous wavelength 403 nm laser illumination. The insets show the real-color photographs of a typical CsPbX₃ square microcrystal, which exhibit bright blue, green, and red emissions, respectively. **Figure 3B,E,H** illustrates the corresponding photoluminescence (PL) spectra and far-field emission pictures of these CsPbX₃ microcrystals. Under focused laser excitation, strong emissions with luminescence peaks at the wavelength of 425, 531, and 706 nm are observed for CsPbX₃ with X = Cl, Br, and I, respectively.

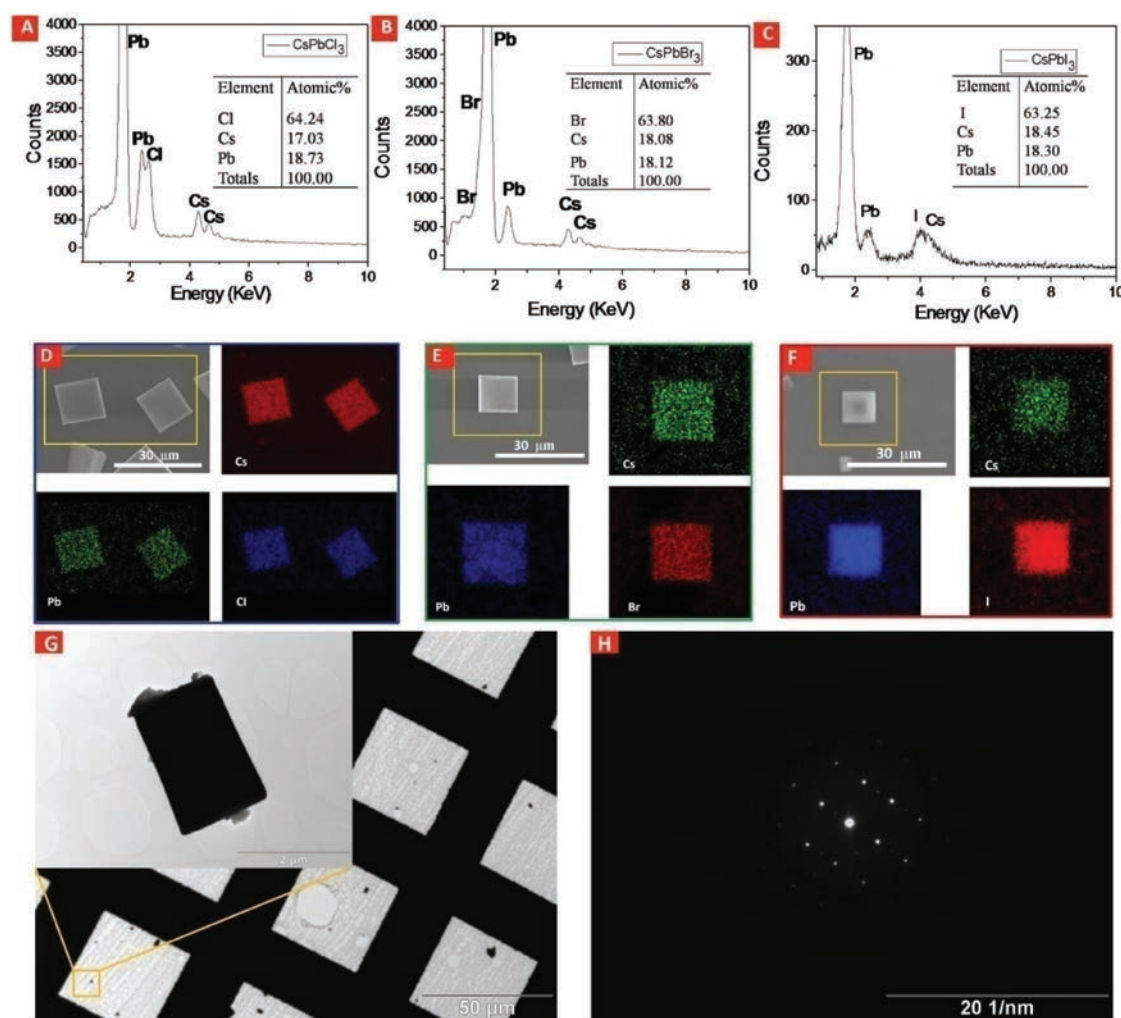


Figure 2. Compositional analysis of CsPbX₃ (X = Cl, Br, I) structures. A–C) EDS spectra of CsPbCl₃, CsPbBr₃, and CsPbI₃ microcrystals, respectively. The insets are the corresponding atomic ratios of the crystals. D–F) Typical SEM images and corresponding elemental maps of the CsPbCl₃, CsPbBr₃, and CsPbI₃ microcrystals. G) A low-magnification TEM image of CsPbBr₃ microcrystals. The microcrystals were randomly dispersed on a copper grid. The inset shows a representative TEM image of a single CsPbBr₃ crystal. H) The corresponding SAED pattern of the CsPbBr₃ microcrystal shown in the inset of (G).

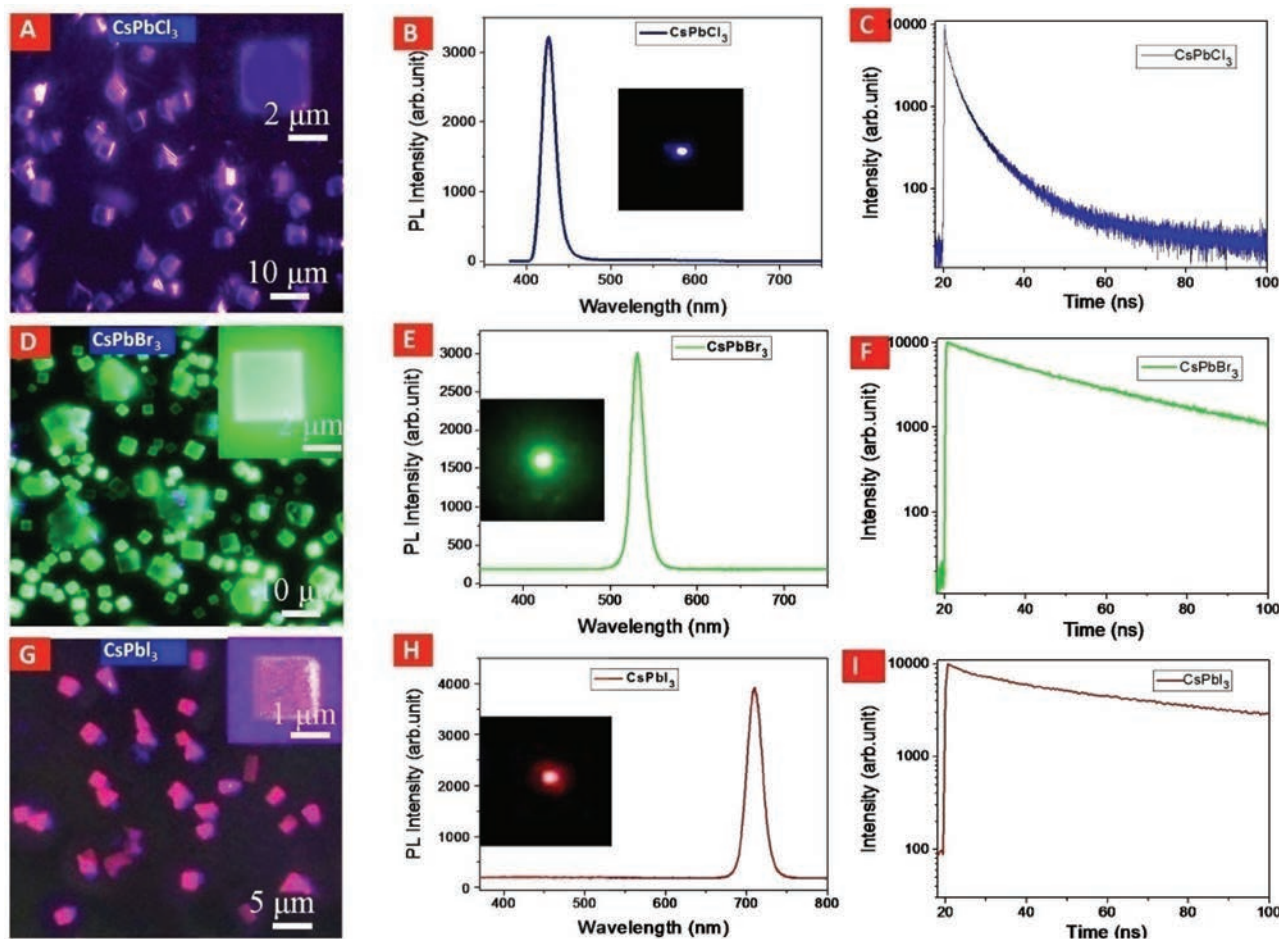


Figure 3. Top-view real-color PL images of the as-grown A) CsPbCl₃, D) CsPbBr₃, and G) CsPbI₃ microcrystals excited by a 403 nm unfocused laser. The insets show the enlarged photographs of individual crystals. B,E,H) PL spectra collected from the CsPbCl₃, CsPbBr₃, and CsPbI₃ microcrystals, respectively: the insets show the corresponding far-field emission pictures from the original substrate. C,F,I) Time-resolved PL spectra of the perovskite microstructures (CsPbX₃, X = Cl, Br, I), respectively.

It is worth noting that the luminescence peaks are rather sharp with full-width-at-half-maximum (FWHM) peak widths of ≈ 20 nm. These optical properties are consistent with high-quality single crystalline materials as shown in structural analysis results in Figure 2. Carrier lifetimes of the CsPbX₃ microstructures are also obtained from time-resolved PL spectra as shown in Figure 3C,F,I. A short decay time of 3.5 ns is observed for CsPbCl₃ microstructures. However, the lifetimes of CsPbBr₃ and CsPbI₃ are much longer, and they are about 36.9 ns (Figure 3F) and 59.7 ns (Figure 3I), respectively. The lifetimes of these structures are found to vary at different positions on the substrate (see Figure S4 in the Supporting Information), which is probably due to the variation in thickness and size of these perovskite structures on the substrate.^[50,51] In this case, further investigations on single crystals are needed in the future for an in-depth understanding of effects of structural properties on the carrier dynamics of these microstructures.

For practical applications, we propose to use these square-like microstructures of CsPbX₃ as the gain materials and resonant cavities simultaneously for the fabrication of WGM lasers.^[52–54] To validate this concept we use a 355 nm pulsed laser beam focused to ≈ 100 μm by a microscope objective to optically pump

on a CsPbCl₃ microcrystal. The optical signals are then detected in situ by a spectrometer, since a local modulation is often necessary for integrated photonic circuits.^[55,56] Figure 4A plots the pumping power-dependent PL spectra of a single CsPbCl₃ microcrystal with a side length of ≈ 15 μm at room temperature. The microcrystal exhibits broad spontaneous emission bands with the peak centered at 425 nm at a low pumping power density as shown in the right enlarged PL spectrum in Figure 4A. When the pump power was increased to certain levels around 32.7 μJ cm⁻², sharp emission lines started to appear at around 427 nm, indicating that lasing action in this microcavity occurred. At this high pump power, a great majority of photons are emitted from the edge of the microsquare, resulting in a WGM-lasing emission from the microstructure. The left inset in Figure 4A shows the emission images of the CsPbCl₃ microcrystal with the power density below and above the lasing threshold, which intuitively reflect the photon behavior under different excitation states. The middle inset in the figure shows the enlarged PL spectrum with the pump power density of 94.8 μJ cm⁻², in which WGM can be clearly seen to be located on both sides of the peak center.

It is worth mentioning that the FWHM of the lasing mode is 0.48 nm owing to the occurrence of stimulated emission in

the WGM cavity (Figure S5, Supporting Information), which is much narrower than original luminescence peaks (≈ 20 nm). This lasing line width of the dominant emission peak of 0.48 nm is comparable to most previously reported values of 0.26^[20] and 0.49 nm^[17] on perovskite microcavities. Mode hopping does not occur when the laser operates with the increased pumping power density, which suggests that the lasing stabilities for these perovskite microplates are acceptable. The measured mode space $\Delta\lambda$ is 1.27 nm (Figure S5A, Supporting Information), being consistent with the calculated results according to the definition of the mode spacing in a square WGM resonator described with the analytical formula^[57]

$$\Delta\lambda = \lambda^2 / 2\sqrt{2}Ln_g \quad (1)$$

where $\Delta\lambda$ is the mode spacing, L is the side length of the microsquare, n_g is the refractive index, and λ is the emission wavelength. The calculated spacing is 1.25 nm from this equation.

Luminescence intensity of the lasing peaks from the microcrystals as a function of the pumping power density is also displayed in Figure 4B; it clearly exhibits a linearly increasing trend when the power density is increased above a threshold of $\approx 32 \mu\text{J cm}^{-2}$. In this case, the blue–green–red peaks lasing from microcrystals of CsPbX_3 perovskites with different anions ($X = \text{Cl, Br, I}$) were successfully realized at room temperature, as shown in Figure 4C. Pumping power-dependent PL spectra of single CsPbBr_3 and CsPbI_3 microcrystals at room temperature are given in Figures S6 and S7 (Supporting Information), in which the lasing peaks are located at 534.3 and 708.6 nm, respectively, with thresholds of about 16.7 and $28.4 \mu\text{J cm}^{-2}$. These threshold values are slightly higher than those found for CsPbX_3 nanowires by Fu et al. ($2.8\text{--}9 \mu\text{J cm}^{-2}$)^[19] and Zhou et al. ($2.1\text{--}15 \mu\text{J cm}^{-2}$)^[20] for F–P lasing. Comparing to the lasing threshold of $125 \mu\text{J cm}^{-2}$ reported by Wang et al. for CsPbBr_3 perovskite platelet,^[45] our lasing thresholds are substantially lower. Notably, all the multicolor lasing peaks have a tiny redshift of ≈ 16 meV as compared with the corresponding spontaneous emission peaks, owing to the self-absorption process during the light transmission and oscillation. All results clearly demonstrate that the microstructures can confine tri-color emissions, which can provide the necessary model materials for white-light emitters.

At present, the white-light emission based on nanostructures of a single perovskite crystal still faces enormous challenges.^[22] Here, we propose a white-light-emitting device based on perovskite structures grown on sapphire substrates. Figure 5A depicts the schematic diagram of the experimental configuration for the measurement of the optically pumped PL spectra. The excitation laser beam (403 nm output) was focused (spot size, $\approx 200 \mu\text{m}$) by an objective and then pumped locally on the microstructures grown on sapphire substrates. The local optical signal is then detected by a spectrometer, and the far-field optical image is recorded by a charge coupled device (CCD) color camera. Figures 5B–D shows the real-color emission photographs and PL spectra of the perovskite CsPbX_3 structures, respectively. Blue (425 nm; Figure 5B), green (531 nm; Figure 5C), and red (706 nm; Figure 5D) emissions with the high fluorescence efficiency on the thin sapphire substrate can be clearly seen. This

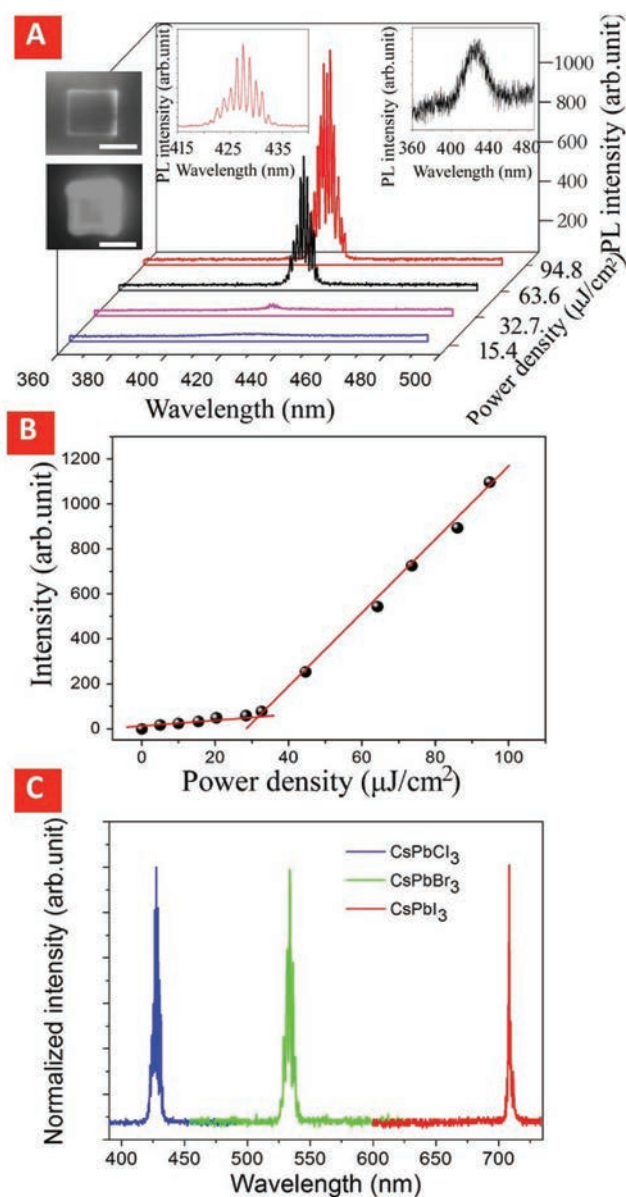


Figure 4. Stimulated emission spectra of CsPbX_3 ($X = \text{Cl, Br, I}$) perovskite microcrystals. A) Pumping power-dependent PL spectra of a single CsPbCl_3 microcrystal at room temperature. The left insets show PL image of the microcrystals with the power density of 15.4 and $94.8 \mu\text{J cm}^{-2}$ (scale bar is $10 \mu\text{m}$), while the middle and right insets show the enlarged PL spectra with the pump power density of 94.8 and $15.4 \mu\text{J cm}^{-2}$, respectively. B) Pumping power-dependent PL intensity of the lasing peaks. C) Red, green, and blue lasing from the perovskite microstructures (CsPbX_3 , $X = \text{Cl, Br, I}$).

high fluorescence efficiency may arise from the excellent crystallinity of the materials. At the same time, the sapphire substrate may also contribute to the optical transmission and diffusion of the guided light. A comparison of the luminescence intensity of perovskite CsPbBr_3 microcrystals grown on SiO_2/Si and sapphire substrates demonstrated that the emission intensity of microcrystals on sapphire is 1.2 times larger than that grown on the SiO_2/Si under the same excitation conditions (Figure S8, Supporting Information). More importantly, our perovskite

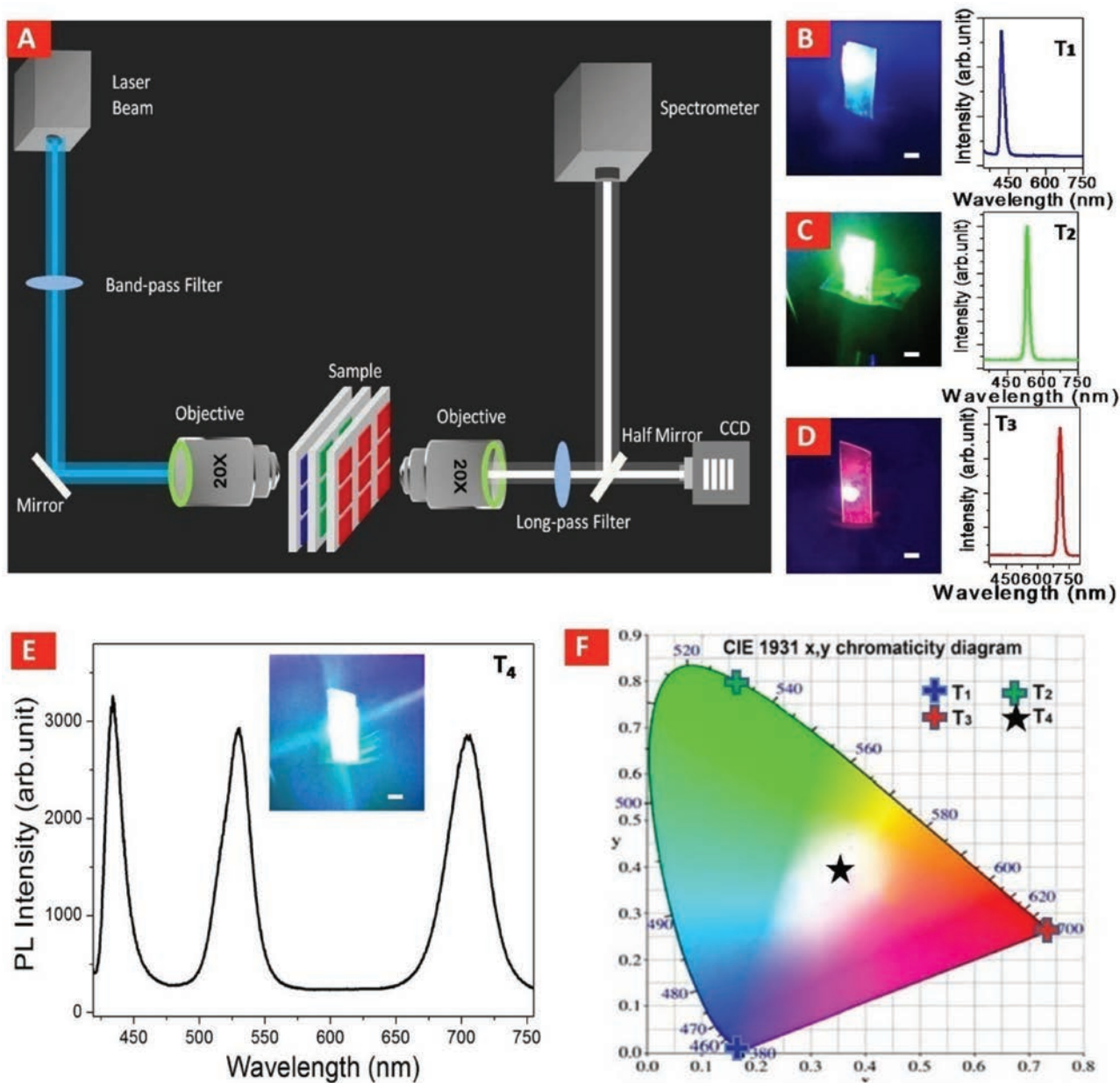


Figure 5. Optical investigations of CsPbX_3 ($X = \text{Cl, Br, I}$) perovskite microcrystals. A) A schematic diagram of the optical setup of the PL measurement. B–D) PL spectra and corresponding far-field emission images of the perovskite (CsPbX_3 , $X = \text{Cl, Br, I}$) microcrystals grown on sapphire at room temperature, respectively. A 1 mm scale bar is shown on each image. E) PL spectrum and far-field emission picture of the tri-layer sapphire chips with CsPbX_3 ($X = \text{Cl, Br, I}$) crystals. F) CIE chromaticity diagram of the four different samples calculated using the obtained PL spectra shown in T_1 – T_4 .

microcrystals exhibit high stability under the laser excitation. For example, the CsPbBr_3 microcrystals, which were grown on sapphire substrate, were illuminated by a focused 403 nm laser in an air environment. After the irradiation for several cycles, the emission intensity of our sample experienced no noticeable attenuation, as shown in Figure S9 (Supporting Information).

Finally, multiwavelength emissions from these perovskite CsPbX_3 microstructures were also investigated at room temperature. CsPbX_3 microstructures with different anions were grown on separate sapphire substrates and then they were stacked together. Since microcrystals were grown randomly on

sapphire substrates (see Figure S8, Supporting Information), there is sufficient space between microcrystals for the pump laser to pass through the sapphire substrate on top and illuminate the microcrystals underneath. Figure S10A,B (Supporting Information) plots the PL spectra of dual-layer sapphire chips with CsPbX_3 ($X = \text{Cl}$ and Br or $X = \text{Br}$ & I) crystals, respectively. Dual-wavelength emission with the peaks at 425 and 531 nm for $X = \text{Cl}$ and Br (Figure S10A, Supporting Information) and 531 and 706 nm for $X = \text{Br}$ and I (Figure S10B, Supporting Information) is demonstrated coming from the dual-layer sapphire chips with various perovskites, respectively. Figure 5E

shows the white-light emission of the tri-layer sapphire chips with CsPbX₃ (X = Cl, Br, I) microcrystals. The three luminescence peaks located at 425, 531, and 706 nm in the PL spectrum are consistent with the observed white-light emission in Figure 5E. Importantly, Figure 5F depicts the Commission Internationale de L'Éclairage (CIE) chromaticity diagram of the four different samples calculated using the obtained PL spectra shown in T₁–T₄. A white-light emission T₄ was located nearly at the center of CIE chromaticity diagram formed by the three typical emissions T₁ (425 nm, blue), T₂ (531 nm, green), and T₃ (706 nm, red). All these results evidently demonstrate that these perovskite microcrystals can be exploited as next-generation integrated full-color display devices.

3. Conclusion

In summary, high-quality metal halide perovskite microcrystals were synthesized by a simple CVD process. Microstructural characterization reveals that all these crystals have a single-crystalline-like structure without any observable defects. Room-temperature optically pumped lasing with red, green, and blue emissions are also successfully realized by WGM oscillator based on these perovskites (CsPbX₃, X = Cl, Br, I) micro-squares. Moreover, for the first time a white-light-emitting device was achieved based on perovskite (CsPbX₃, X = Cl, Br, I) layered structures grown on sapphire. All these findings indicate that these metal halide perovskite materials have the promising potency for the utilization in integrated full-color display devices, and other photonic elements throughout the entire visible range.

4. Experimental Section

Material Preparation: Perovskite microstructures were grown via a CVD method. All powder sources and reagents were purchased from Alfa Aesar. The setup includes a horizontal furnace with a quartz tube (inner diameter = 45 mm, length = 150 cm). Before the growth, CsX and PbX₂ (X = Cl, Br, I) were mixed in a boron nitride boat, with a mole ratio of 1:1, located at the center of the furnace. SiO₂/Si or sapphire substrate pieces were placed at the downstream to collect the product. Before heating up, an argon gas flow was introduced into the tube at 100 sccm for half an hour to purge out any residual air of the tube. After that, the furnace was heated to temperatures of 620, 620, and 580 °C at a rate of 35 °C min⁻¹ to grow the CsPbCl₃, CsPbBr₃, and CsPbI₃, respectively. At the same time, the tube pressure was fixed at 4.8, 4.8, and 5.2 torr for the growth of the three materials and the growth lasted for a duration of 30 min. After the growth, the furnace was naturally cooled to room temperature.

Optical Characterization: PL measurements were performed by a home-built optical system. A 403 nm laser beam was focused to ≈80 μm and pumped on the perovskite microstructures by a microscope objective. A CCD camera was used to record the far-field optical photographs and real-color images as shown in Figure 5A. Stimulated emission experiments were performed by another confocal optical system. A 355 nm pulse laser was focused to ≈100 μm and then pumped locally onto the microcrystals. Optical images and PL spectra were recorded by a noncolor CCD camera and Ocean Optics Spectrometer (USB 4000), respectively. The PLQY was measured using a home-made intergraded sphere to quantify the absorbed photons and emitted photons. The photoluminescence quantum yield (PLQY) measured for CsPbX₃ (X = Cl, Br, I) perovskite samples is 5.9%, 10.0%, and 8.3%, respectively.

Supporting Information

Supporting Information is available from the Wiley Online Library or from the author.

Acknowledgements

The authors thank Professor Wallace C. H. Choy (The University of Hong Kong) for access to his laboratory to perform time-resolved spectral characterization of the microstructures. This work was financially supported by CityU SGP (Grant No. 9380076), the National Natural Science Foundation of China (Grant Nos. 51602276, 51672229, 61574122, and 11604280), the Hong Kong Scholars Program (Grant No. XJ2015013), the General Research Fund of the Research Grants Council of Hong Kong SAR, China (CityU 11275916), the Nan Hu Young Scholar Supporting Program of XYNU, Key research program in the University of Henan Province (Grant No. 17A140028), and the Science and Technology Project of Henan Province (Grant No. 172102210458).

Conflict of Interest

The authors declare no conflict of interest.

Keywords

microstructures, perovskites, photonics, WGM lasers, white-light emission

Received: September 20, 2017

Revised: November 20, 2017

Published online: December 27, 2017

- [1] F. Fan, S. Turkdogan, Z. C. Liu, D. Shelhammer, C. Z. Ning, *Nanotechnol.* **2015**, *10*, 796.
- [2] X. J. Zhuang, P. F. Guo, Q. L. Zhang, H. W. Liu, D. Li, W. Hu, X. L. Zhu, H. Zhou, A. L. Pan, *Nano Res.* **2016**, *9*, 933.
- [3] Y. Lu, F. X. Gu, C. Meng, H. K. Yu, Y. G. Ma, W. Fang, L. M. Tong, *Opt. Express* **2013**, *21*, 22314.
- [4] J. Y. Tsao, M. E. Coltrin, M. H. Crawford, J. A. Simmons, *Proc. IEEE* **2010**, *98*, 1162.
- [5] K. Seo, T. Lim, S. Kim, H. L. Park, S. Ju, *Nanotechnology* **2010**, *21*, 255201.
- [6] H. P. T. Nguyen, S. Zhang, K. Cui, X. Han, S. Fatholoulumi, M. Couillard, G. A. Botton, Z. Mi, *Nano Lett.* **2011**, *11*, 1919.
- [7] H. W. Lin, Y. J. Lu, H. Y. Chen, H. M. Lee, S. Gwo, *Appl. Phys. Lett.* **2010**, *97*, 073101.
- [8] Z. Y. Yang, J. Y. Xu, P. Wang, X. J. Zhuang, A. L. Pan, L. M. Tong, *Nano Lett.* **2011**, *11*, 5085.
- [9] Y. Ding, Q. Yang, X. Guo, S. S. Wang, F. X. Gu, J. Fu, Q. Wan, J. P. Cheng, L. M. Tong, *Opt. Express* **2009**, *17*, 21813.
- [10] S. Sapra, S. Mayilo, T. A. Klar, A. L. Rogach, J. Feldmann, *Adv. Mater.* **2007**, *19*, 569.
- [11] R. Mirhosseini, M. F. Schubert, S. Chhajed, J. Cho, J. K. Kim, E. F. Schubert, *Opt. Express* **2009**, *17*, 10807.
- [12] M. H. Crawford, *IEEE J. Sel. Top. Quantum Electron.* **2009**, *15*, 1028.
- [13] S. Ha, R. Su, J. Xing, Q. Zhang, Q. H. Xiong, *Chem. Sci.* **2017**, *8*, 2522.
- [14] N. J. Jeon, J. H. Noh, W. S. Yang, Y. C. Kim, S. Ryu, J. Seo, S. I. Seok, *Nature* **2015**, *517*, 476.
- [15] Y. Wang, X. M. Li, X. Zhao, L. Xiao, H. B. Zeng, H. D. Sun, *Nano Lett.* **2016**, *16*, 448.

- [16] Q. Zhang, R. Su, X. F. Liu, J. Xing, T. C. Sum, Q. H. Xiong, *Adv. Funct. Mater.* **2016**, *26*, 6238.
- [17] Y. P. Fu, T. Wu, J. Wang, J. Y. Zhai, M. J. Shearer, Y. Z. Zhao, R. J. Hamers, E. Kan, K. M. Deng, X. Y. Zhu, S. Jin, *Nano Lett.* **2017**, *17*, 4405.
- [18] S. T. Ha, C. Shen, J. Zhang, Q. H. Xiong, *Nat. Photonics* **2016**, *10*, 115.
- [19] Y. P. Fu, H. M. Zhu, C. C. Stoumpos, Q. Ding, J. Wang, M. G. Kanatzidis, X. Y. Zhu, S. Jin, *ACS Nano* **2016**, *10*, 7963.
- [20] H. Zhou, S. P. Yuan, X. X. Wang, T. Xu, X. Wang, H. L. Li, W. H. Zheng, P. Fan, Y. Y. Li, L. T. Sun, A. L. Pan, *ACS Nano* **2017**, *11*, 1189.
- [21] Q. A. Akkerman, V. D'Innocenzo, S. Accornero, A. Scarpellini, A. Petrozza, M. Prato, L. Manna, *J. Am. Chem. Soc.* **2015**, *137*, 10276.
- [22] L. T. Dou, M. L. Lai, C. S. Kley, Y. M. Yang, C. G. Bischak, D. D. Zhang, S. W. Eaton, N. S. Ginsberg, P. D. Yang, *Proc. Natl. Acad. Sci. USA* **2017**, *114*, 7216.
- [23] L. Dimesso, M. Wussler, T. Mayer, E. Mankel, W. Jaegermann, *AIMS Mater. Sci.* **2016**, *3*, 737.
- [24] G. Xing, N. Mathews, S. S. Lim, N. Yantara, X. F. Liu, D. Sabba, M. Grätzel, S. Mhaisalkar, T. C. Sum, *Nat. Mater.* **2014**, *13*, 476.
- [25] Q. Zhang, S. T. Ha, X. Liu, T. C. Sum, Q. H. Xiong, *Nano Lett.* **2014**, *14*, 5995.
- [26] H. Zhu, Y. P. Fu, F. Meng, X. X. Wu, Z. Z. Gong, Q. Ding, M. V. Gustafsson, M. T. Trinh, S. Jin, X. Y. Zhu, *Nat. Mater.* **2015**, *14*, 636.
- [27] A. Kojima, K. Teshima, Y. Shirai, T. Miyasaka, *J. Am. Chem. Soc.* **2009**, *131*, 6050.
- [28] J. Burschka, N. Pellet, S. Moon, R. Baker, P. Gao, M. K. Nazeeruddin, M. Grätzel, *Nature* **2013**, *499*, 316.
- [29] M. Liu, M. B. Johnston, H. J. Snaith, *Nature* **2013**, *501*, 395.
- [30] H. Tsai, W. Nie, J. Blancon, C. C. Stoumpos, R. Asadpour, B. Harutyunyan, A. J. Neukirch, R. Verduzco, J. J. Crochet, S. Tretiak, L. Pedesseau, J. Even, M. A. Alam, G. Gupta, J. Lou, P. M. Ajayan, M. J. Bedzyk, M. G. Kanatzidis, A. D. Mohite, *Nature* **2016**, *536*, 312.
- [31] Z. K. Tan, R. S. Moghaddam, M. L. Lai, P. Docampo, R. Higler, F. Deschler, M. Price, A. Sadhanala, L. M. Pazos, D. Credgington, F. Hanusch, T. Bein, H. J. Snaith, R. H. Friend, *Nat. Nanotechnol.* **2014**, *9*, 687.
- [32] J. Xing, F. Yan, Y. W. Zhao, S. Chen, H. K. Yu, Q. Zhang, R. G. Zeng, H. V. Demir, X. W. Sun, A. Huan, Q. H. Xiong, *ACS Nano* **2016**, *10*, 6623.
- [33] M. J. Yuan, L. N. Quan, R. Comin, G. Walters, R. Sabatini, O. Voznyy, S. Hoogland, Y. B. Zhao, E. M. Beauregard, P. Kanjanaboos, Z. H. Lu, D. H. Kim, E. H. Sargent, *Nat. Nanotechnol.* **2016**, *11*, 872.
- [34] Q. A. Akkerman, V. D'Innocenzo, S. Accornero, A. Scarpellini, A. Petrozza, M. Prato, L. Manna, *J. Am. Chem. Soc.* **2015**, *137*, 10276.
- [35] G. Nedelcu, L. Protesescu, S. Yakunin, M. I. Bodnarchuk, M. J. Grotevent, M. V. Kovalenko, *Nano Lett.* **2015**, *15*, 5635.
- [36] M. C. Weidman, M. Seitz, S. D. Stranks, W. A. Tisdale, *ACS Nano* **2016**, *10*, 7830.
- [37] I. Lignos, S. Stavrakis, G. Nedelcu, L. Protesescu, A. J. deMello, M. V. Kovalenko, *Nano Lett.* **2016**, *16*, 1869.
- [38] L. Protesescu, S. Yakunin, M. I. Bodnarchuk, F. Krieg, R. Caputo, C. H. Hendon, R. X. Yang, A. Walsh, M. V. Kovalenko, *Nano Lett.* **2015**, *15*, 3692.
- [39] P. F. Guo, J. Y. Xu, K. Gong, X. Shen, Y. Lu, Y. Qiu, J. Q. Xu, Z. J. Zou, C. L. Wang, H. L. Yan, Y. S. Luo, A. L. Pan, H. Zhang, J. C. Ho, K. M. Yu, *ACS Nano* **2016**, *10*, 8474.
- [40] J. Hu, Y. Bando, Z. Liu, T. Sekiguchi, D. Golberg, J. Zhan, *J. Am. Chem. Soc.* **2003**, *125*, 11306.
- [41] M. Y. Lu, J. Song, M. Lu, C. Lee, L. Chen, Z. L. Wang, *ACS Nano* **2009**, *3*, 357.
- [42] P. F. Guo, X. J. Zhuang, J. Y. Xu, Q. L. Zhang, W. Hu, X. L. Zhu, X. X. Wang, Q. Wan, P. B. He, H. Zhou, A. L. Pan, *Nano Lett.* **2013**, *13*, 1251.
- [43] S. T. Ha, X. F. Liu, Q. Zhang, D. Giovanni, T. C. Sum, Q. H. Xiong, *Adv. Opt. Mater.* **2014**, *2*, 838.
- [44] K. Park, J. W. Lee, J. D. Kim, N. S. Han, D. M. Jang, S. Jeong, J. Park, J. K. Song, *J. Phys. Chem. Lett.* **2016**, *7*, 3703.
- [45] Y. L. Wang, X. Guan, D. H. Li, H. Cheng, X. D. Duan, Z. Y. Lin, X. F. Duan, *Nano Res.* **2017**, *10*, 1223.
- [46] M. R. Leyden, L. Q. Meng, Y. Jiang, L. K. Ono, L. B. Qiu, E. J. Juarez-Perez, C. J. Qin, C. Adachi, Y. B. Qi, *J. Phys. Chem. Lett.* **2017**, *8*, 3193.
- [47] M. R. Leyden, L. K. Ono, S. R. Raga, Y. Kato, S. H. Wang, Y. B. Qi, *J. Mater. Chem. A* **2014**, *2*, 18742.
- [48] C. K. Moller, *Nature* **1958**, *182*, 1436.
- [49] Y. Fujii, S. Hoshino, Y. Yamada, G. Shirane, *Phys. Rev. B* **1974**, *9*, 4549.
- [50] Y. Li, W. B. Yan, Y. L. Li, S. F. Wang, W. Wang, Z. Q. Bian, L. X. Xiao, Q. H. Gong, *Sci. Rep.* **2015**, *5*, 14485.
- [51] S. P. Malyukov, A. V. Sayenko, A. V. Ivanova, *IOP Conf. Ser.: Mater. Sci. Eng.* **2016**, *151*, 012033.
- [52] X. F. Liu, S. T. Ha, Q. Zhang, M. Mata, C. Magen, J. Arbiol, T. C. Sum, Q. H. Xiong, *ACS Nano* **2015**, *9*, 687.
- [53] H. Baek, C. H. Lee, K. Chung, G. C. Yi, *Nano Lett.* **2013**, *13*, 2782.
- [54] H. Y. Dong, C. H. Zhang, X. Q. Lin, Z. H. Zhou, J. N. Yao, Y. S. Zhao, *Nano Lett.* **2017**, *17*, 91.
- [55] J. B. Li, C. Meng, Y. Liu, X. Q. Wu, Y. Z. Lu, Y. Ye, L. Dai, L. M. Tong, X. Liu, Q. Yang, *Adv. Mater.* **2013**, *25*, 833.
- [56] X. F. Liu, Q. Zhang, Q. H. Xiong, T. C. Sum, *Nano Lett.* **2013**, *13*, 1080.
- [57] A. K. Bhowmik, *Appl. Opt.* **2000**, *39*, 3071.